

Gamma ray emission from SNR RX J1713.7-3946 and the origin of galactic cosmic rays

G. Morlino^{1,2}, E. Amato¹, and P. Blasi^{1,2},

¹INAF-Osservatorio Astronomico di Arcetri, Largo E. Fermi, 5, 50125 Firenze, Italy

²Center for Particle Astrophysics, Fermi National Accelerator Laboratory, Batavia, IL, USA

Accepted | Received |

ABSTRACT

We calculate the flux of non-thermal radiations from the supernova remnant (SNR) RX J1713.7-3946 in the context of the non-linear theory of particle acceleration at shocks, which allows us to take into account self-consistently the dynamical reaction of the accelerated particles, the generation of magnetic fields in the shock proximity and the dynamical reaction of the magnetic field on the plasma. When the fraction of particles which get accelerated is of order 10^{-4} , we find that the strength of the magnetic field obtained as a result of streaming instability induced by cosmic rays is compatible with the interpretation of the X-ray emitting filaments being produced by strong synchrotron losses in 100 G magnetic fields. The maximum energy of accelerated protons is $> 10^5$ GeV. If the X-ray filaments are explained in alternative ways, the constraint on the magnetic field downstream of the shock disappears and the HESS data can be marginally fit with ICS of relativistic electrons of a complex population of photons, tailored to comprise CMB and ambient IR/Optical photons. The fit, typically poor at the highest energies, requires a large density of target photons within the remnant; only a fraction of order 10^{-6} of the background particles gets accelerated; the local magnetic field is of order 20 G and the maximum energy of protons is much lower than the knee energy. Current HESS gamma ray observations combined with recent X-ray observations by Suzaku do not allow as yet to draw a definitive conclusion on whether RX J1713.7-3946 is an efficient cosmic ray accelerator, although at the present time a hadronic interpretation of HESS data seems more likely. We discuss the implications of our results for the GLAST gamma ray telescope, which should be able to discriminate the two scenarios discussed above, by observing the shape of the gamma ray spectrum at lower energies.

Key words: acceleration of particles { nonthermal emission - magnetic field amplification { object: RX J1713.7-3946

1 INTRODUCTION

The detection of high energy gamma rays from supernova remnants has long been considered as the most promising tool to test the supernova paradigm for the origin of the bulk of cosmic rays observed at the Earth. Several supernova remnants (SNRs) have now been detected in gamma rays, while useful upper limits have been obtained for several others (see Tatischev (2008) and references therein for a recent review of observations and their implications). The question now to be answered is whether such emissions can be reliably considered as a proof of the acceleration of hadronic parti-

cles (cosmic rays) or if they should be rather interpreted as the result of radiative losses of relativistic electrons. This goal can be achieved by investigating the following aspects: 1) spectrum of the gamma ray emission combined with the spectrum of X-rays (and possibly radio emission); 2) high energy cutoff of the gamma ray emission; 3) morphology of the emission.

Here we specialize our calculations to the SNR RX J1713.7-3946.

For this remnant, the HESS Cherenkov gamma ray telescope has measured a spectrum extending to 100 TeV, although a power law spectrum with an exponential cutoff at E^{max} leads to a best fit with $E^{\text{max}} = 10$ TeV (Aharonian et al. 2006, 2007). If this emission is due to decay of neutral pions produced by nuclear collisions of relativistic protons with some target gas in the shock vicinity,

? E-mail: morlino@arcetri.astro.it

y E-mail: amato@arcetri.astro.it

z E-mail: blasi@arcetri.astro.it; blasi@fnal.gov

then this would imply a cutoff in the spectrum of accelerated protons at ~ 100 TeV, roughly a factor of 30 short of the knee. It is worth keeping in mind that in an expanding SNR the highest cosmic ray energy is expected to be reached around the beginning of the Sedov phase. Before and after that time the maximum energy of accelerated particles does not need to be as high as the knee energy. Moreover, different SNRs might accelerate to different maximum energies because of the different environment in which they explode. In this sense it is only natural that most SNRs do not show proton acceleration up to the energy of the knee.

The strength and topology of the magnetic field in the acceleration/radiation region regulate the efficiency of particle acceleration (nuclei and electrons) and the radiation losses of electrons. The recent detection of narrow X-ray bright rims in several SNRs (Bamba et al. 2003, 2005; Lazendic et al. 2003, 2004; Vink & Laming 2003) has allowed to infer the strength of the field, if the thickness of the rim is interpreted as the synchrotron loss length of the radiating electrons (Ballet 2006). Typical values of 50–1000 G have been inferred, which suggest efficient magnetic field amplification in the shock region. One more argument in favor of strong magnetic fields was made by Uchiyam et al. (2007) who interpreted the rapid time variability (of the order of few years) observed in some X-ray emitting regions of RX J1713.7–3946 as due to rapid synchrotron cooling. The field strength inferred based on this interpretation is as high as ~ 1 mG. The same effect was also observed in some knots of Cassiopeia A (Uchiyam et al. & Aharonian 2008).

There is however a large source of ambiguity in that the narrow thickness of the X-ray rim might be due to damping of the magnetic field (for instance due to wave-wave non-linear coupling) (Pohl et al. 2005). In this case the magnetic field inferred by assuming that the rims are due to severe synchrotron losses might be overestimated. We discuss this issue at several points throughout the paper.

Magnetic field amplification could result from turbulent amplification (Giacomini & Jokipii 2007) or from cosmic ray induced streaming instability. An open question is whether the large magnetic fields present in the X-ray rims are widespread throughout the remnant or are rather confined in thin filaments with a relatively small filling factor (this would be the case if damping plays a role downstream of the shock). This difference might have important consequences on the interpretation of the observed non-thermal emission from SNRs, as we discuss below.

Interestingly enough, the magnetic field strength inferred from X-ray observations is of the same order of magnitude as that required by the theory of shock acceleration in order to account for particle acceleration up to the knee region, provided the diffusion coefficient is Bohm-like.

From the theoretical point of view, a major improvement has been achieved in the last few years in that the calculations are carried out in the context of the so-called non-linear theory of particle acceleration. This theory allows us to calculate the spectrum and spatial distribution of accelerated particles around the shock, their dynamical reaction on the shock and the magnetic field amplification that cosmic rays induce due to streaming instability.

Although the non-linear theory has been previously applied to SNRs, this paper improves on previous attempts in two major aspects: 1) the magnetic field in the shock region

is calculated from streaming instability and from conservation equations instead of being inserted ad hoc in such a way to fit the X-ray observations; 2) we include the dynamical reaction of the turbulent magnetic field on the shock, which is a very important effect in shaping the shock precursor (Caprioli et al. (2008a,b)).

The first point is of crucial importance in that it allows us to achieve a unified picture of the spectra of X-ray and gamma-ray emission, together with the morphology of the X-ray emission, the strength of the magnetic field and finally the diffusion properties of the accelerated particles. Inclusion of the dynamical reaction of the field, then, as showed by Caprioli et al. (2008a), leads to a substantial reduction of the compression in the precursor, thereby also reducing the concavity of the spectrum of accelerated particles (Caprioli et al. (2008b)). A reduced concavity of the spectrum should also be expected as a result of the enhanced velocity of the scattering centers when the magnetic field is amplified (see for instance Zirakashvili & Ptuskin (2000)).

The large values of the magnetic field strength inferred from X-ray observations and confirmed by our calculations clearly favor a hadronic interpretation of the observed gamma-ray emission, because a subdominant population of electrons is sufficient to explain the spectrum and intensity of the observed X-ray emission, but is insufficient to produce the observed gamma-ray emission through inverse Compton scattering (ICS) on the CMB and infrared/optical photons (IR+Opt). The issue of whether the large fields are present in large fractions of the remnant volume or are rather confined in narrow filaments, remains however an open issue.

For this reason we also investigate the possibility that the filaments have some alternative explanation, so that there is no constraint on the strength of the magnetic field downstream. We still use our non-linear calculations to derive the spectra of accelerated protons and electrons, but force the injection to be low enough to avoid large magnetic fields produced by streaming instability. We find that a marginal fit to the gamma-ray and X-ray data is possible, although a large density of IR photons needs to be assumed inside the remnant. The fit to the highest energy part of the gamma-ray spectrum is not as good as for the hadronic interpretation.

The general conclusion we draw is that although there are numerous indications that the observed gamma-ray spectrum may be of hadronic origin, a clear answer on this point may only come from: a) the extension of the gamma-ray observations to lower energies, and b) the detection of high energy neutrinos, which would be produced in the same hadronic interactions (Orino et al. 2008).

The paper is organized as follows: in §2 we discuss in some detail the general lines of the calculations we carry out, including the non-linear theory of particle acceleration, the magnetic field amplification and the different channels of non-thermal emissions. In §3 we discuss the results we obtain by specializing the calculations to the case of the SNR RX J1713.7–3946. We conclude in §4.

2 DESCRIPTION OF THE CALCULATIONS

In this section we discuss the technical aspects of the calculations we carry out, with special attention for the compu-

tation of the spectra of protons and electrons, the magnetic field amplification and the radiation processes that we include.

2.1 Spectra of accelerated protons and electrons

The dynamics of the shock region is dominated by accelerated protons, while electrons are accelerated in the shock environment generated by protons. In this sense the non-linearity of the problem is limited to the proton component, which also generates the local magnetic field by exciting a streaming instability. The spectrum of accelerated protons is computed using the method of Amato & Blasi (2005). The acceleration time in the presence of a precursor was determined by Blasi et al. (2007), and we adopt that calculation. It was found there (and later confirmed for the parameters of RX J1713.7-3946 by Ellison (2008)) that the precursor reduces the maximum energy compared with the naive prediction of the test-particle theory with the same value of the magnetic field upstream of the subshock.

The maximum momentum is first calculated using as a condition the equality between the acceleration time and the age of the SNR. However we also illustrate our results in the case in which the maximum momentum is determined by the finite size of the accelerator. The diffusion coefficient is chosen to be Bohm-like in the magnetic field generated through streaming instability (see x 2.2). Since the magnetic field depends on the location in the precursor, the diffusion coefficient is also a function of space: $D(p; x) = (1/3)pc^2 = eB(x)$. The two conditions mentioned above read:

$$t_{acc}(p_{max}) = t_{SNR}; \quad \frac{D(p_{max})}{u_0} = R_{SNR}; \quad (1)$$

where $\alpha < 1$ is the fraction of the shell radius (R_{SNR}) where the escape of particles at p_{max} occurs.

Although the basic structure of the calculation is the same proposed by Amato & Blasi (2005) and Amato & Blasi (2006), the crucial new aspect taken into account here is the dynamical reaction of the self-generated magnetic field. We introduce this effect following the treatment of Caprioli et al. (2008a) and Caprioli et al. (2008b): the conservation equations at the shock and in the precursor are modified so as to include the magnetic contribution. The compression factor at the subshock, R_{sub} , and the total compression factor, R_{tot} , are deeply affected by this change, in that the ratio $R_{tot} = R_{sub}$ (the compression factor in the precursor), decreases when the amplified magnetic field contributes a pressure which is comparable with the pressure of the thermal gas upstream. In turn this reflects in spectra of accelerated particles which are closer to power laws, though a concavity remains visible (Caprioli et al. 2008b), as we discuss below.

The normalization of the proton spectrum is an output of our non linear calculation, once a recipe for injection has been established. Following Blasi et al. (2005), particles are injected immediately downstream of the subshock. The fraction of gas particles crossing the shock from downstream to upstream, η_{inj} , can be written as

$$\eta_{inj} = 4 = 3^{\frac{p}{p_{th,2}}} - (R_{sub} - 1)^3 e^{-\frac{p}{p_{th,2}}}; \quad (2)$$

Here $\frac{p}{p_{th,2}}$ is defined by the relation $p_{th,j} = p_{th,2}$, where $p_{th,2}$ is the momentum of the thermal particles downstream.

parameterizes the poorly known microphysics of the injection process, but one should stress that $p_{th,2}$ is an output of the problem: as a result, the injection efficiency is affected by the dynamical reaction exerted by the accelerated particles and by the amplified magnetic field.

The spectrum of accelerated electrons at the shock, $f_{e,0}(p)$, is easy to calculate for $p \leq p_{max}$, with p_{max} the maximum electron momentum. In fact the slope of the electron spectrum at given momentum p is the same as the slope of the proton spectrum at the same momentum, assuming that both electrons and protons experience the same diffusion coefficient. The relative normalization of the two spectra is unconstrained a priori, while the normalization of the proton spectrum, as stressed above, is an output of our non linear calculation.

The maximum energy of electrons is determined by equating the acceleration time with the minimum between the time for energy losses and the age of the remnant. The loss time of electrons over a cycle of shock crossing needs to be weighed by the residence times upstream and downstream, therefore the condition for the maximum momentum, in the loss dominated case, can be written as:

$$t_{acc}(p) = [\tau_{11}(B_1; p) + \tau_{12}(B_2; p)] \frac{\tau_{e,1}(p)}{\tau_{11}(B_1; p)} + \frac{\tau_{e,2}(p)}{\tau_{12}(B_2; p)}; \quad (3)$$

where τ_i denotes the loss time, and the indexes "1" and "2" refer to quantities measured upstream and downstream respectively. The residence times in the context of non linear theory of particle acceleration can be written explicitly (from Eqs. (25) and (26) of Blasi et al. (2007)). Eq. (3) cannot be solved for p_{max} analytically, contrary to the case of acceleration in the test particle regime. The numerical solution is however easy to obtain with standard techniques.

When only synchrotron losses are important, we can provide an approximate expression for the solution of Eq. (3). We use the function $u_p(p)$ defined as the mean plasma velocity that a particle with momentum p experiences in the precursor region (see Eq. (8) in Amato & Blasi (2005)). The function $U_p(p) = u_p(p)/u_0$ is such that $U_p(p) < 1$ for any momentum. The electron maximum momentum can then be written in an implicit way as:

$$p_{max} = \frac{3}{2} \frac{m_e^3 c^4}{eB_1 r_0} \frac{u_0}{c} U_p(p_{max}) \frac{r}{1 + R_B R_{tot} U_p(p_{max})}; \quad (4)$$

where r_0 is the classical electron radius. One may notice that Eq. (4) reduces to the Eq. (11) of Berezhko & Volk (2006) if one poses $U_p = 1$. Eq. (4) leads to an error of less than 10% with respect to Eq. (3) (but we stress that the results presented in this work are all obtained using Eq. (3)).

The spectrum of electrons at energies around and above p_{max} , namely the shape of the cutoff is harder to calculate in the context of a fully non linear calculation. In the test particle case and for strong shocks the solution has been calculated by Zirakashvili & Aharonian (2007). Since the spectra we find for electrons at $p < p_{max}$ are not far from being power laws with slope -4 , we adopt the modification factor calculated by Zirakashvili & Aharonian (2007) and we write the electron spectrum at the shock in the loss dominated case as:

$$f_{e,0}(p) = K_{ep} f_{p,0}(p) \left(1 + 0.523 (p/p_{max})^{\frac{1}{4}} e^{-p^2/p_{max}^2}\right)^{1/2}; \quad (5)$$

The most important aspect of this expression is the fact that the cutoff is not a simple exponential, which in turn reflects in the shape of the secondary emission radiated by electrons. This important conclusion differs from the numerous calculations previously carried out by other authors, where an exponential cutoff was assumed for the electron spectrum. On the other hand, if the maximum momentum is indeed determined by the age of the remnant, then the cutoff shape is expected to be exponential. The constant K_{ep} accounts for the different normalization between the electron and proton spectrum.

2.2 Magnetic field amplification and compression

The turbulent magnetic field close to the shock can be enhanced by several physical processes. Here we concentrate on the amplification due to streaming instability induced by cosmic rays accelerated at the shock and we show that this mechanism allows us to reproduce the strength of the magnetic fields which are inferred by assuming that the thickness of the X-ray filaments is due to severe synchrotron energy losses. On the other hand, if the filaments are interpreted in a different way, very low efficiencies of proton acceleration are required in order to avoid excessive magnetic field amplification.

The streaming of cosmic rays upstream of a shock excites both resonant (Skilling (1975)) and non-resonant (Bell 2004) modes. The latter modes are expected to dominate for fast shocks, efficiently accelerating cosmic rays, most likely during the free expansion phase of the post-supernova evolution and at the very beginning of the Sedov phase (Amato & Blasi 2008). At any later time, resonantly excited Alfvén waves should account for most of the field amplification in the shock vicinity. Although the predictions of quasi-linear theory should be taken with caution when considering the regime of strongly non-linear field amplification, $B = B_0$, at present no better treatment is possible. The strength of the magnetic field at the position x upstream, $B(x)$, in the absence of damping, can be estimated from the saturation condition, that, for modified shocks, reads (Caprioli et al. (2008b)):

$$p_w(x) = U(x)^{-3/2} p_{w,0} + \frac{1}{4M_{A,0}} \frac{U(x)^2}{U_0^2}; \quad (6)$$

where $p_w(x) = B(x)^2/(8\pi u_0^2)$ is the magnetic pressure normalized to the incoming momentum flux at upstream infinity. In Eq. (6), $U(x) = u(x)/u_0$ and $M_{A,0} = u_0/v_A$ is the Alfvénic Mach number at upstream infinity where only the background magnetic field, B_0 , assumed to be parallel to the shock normal, is present. $p_{w,0}$ accounts for the magnetic pressure due to a pre-existing magnetic turbulence. This term is usually set to zero in the following calculations, unless otherwise specified.

Eq. (6) correctly describes into account the effect of compression in the shock precursor through the term $U(x)^{-3/2}$. For the upstream temperature that we adopt in RX J1713.7-3946 (see below), damping in the upstream region is expected to be negligible.

This expression has been derived for Alfvén waves, therefore the perturbation is perpendicular to B_0 , namely

in the plane of the shock. The magnetic field downstream of the subshock is further enhanced by compression:

$$B_2 = R_{\text{sub}} B_1; \quad (7)$$

where B_1 is the magnetic field immediately upstream of the subshock.

The combined action of cosmic ray induced magnetic field amplification and field compression at the subshock results in a situation in which the magnetic pressure may easily exceed the pressure of the background plasma. As shown by (Caprioli et al. 2008a), this leads to a reduction of the compressibility of the plasma, so that the value of R_{tot} drops compared with the cases in which this dynamical reaction of the magnetic field is ignored. As stressed by Caprioli et al. (2008a) this effect alleviates the need for invoking poorly known processes such as the so-called turbulent heating.

2.3 Radiation produced by accelerated particles

In this section we briefly describe the calculations of the fluxes of nonthermal radiation produced by electrons and protons in the SNR. We concentrate on the following channels: 1) gamma ray production by generation and decay of neutral pions in inelastic pp collisions; 2) synchrotron emission of electrons; 3) ICS of electrons on the CMB and infrared/optical photons in the remnant.

The flux and spectrum of gamma rays from π^0 decay are calculated following the analytical approximations discussed by Kelner et al. (2006).

The cutoff in the gamma ray spectrum resulting from π^0 decay can be written as

$$E_{\gamma,\text{cut}} = 0.15 E_{p,\text{max}}; \quad (8)$$

where $E_{p,\text{max}}$ is the maximum energy of accelerated protons. Qualitatively, the spectrum of gamma rays at energy $E \leq E_{\gamma,\text{cut}}$ reproduces the shape of the parent proton spectrum. The gamma ray spectrum is therefore expected to show some level of concavity, typical of acceleration at cosmic ray modified shocks. At energies lower than the pion mass, the gamma ray spectrum is found to rapidly drop.

Synchrotron emission is produced by accelerated electrons in the magnetic field amplified by streaming cosmic ray protons. The calculation of the synchrotron emission is carried out by using the exact synchrotron kernel (Rybicki & Lightman 1985). The synchrotron spectrum is cut off at a photon energy

$$E_{\text{syn;cut}} = 3 \cdot 10^3 B_{100} \frac{E_{e,\text{max}}^2}{\text{TeV}} \text{ keV}; \quad (9)$$

where B_{100} is the local magnetic field in units of 100 G. It is easy to check that for $E_{e,\text{max}} \leq 10 \text{ TeV}$, the synchrotron emission is cut off in the keV energy range. It is also worth keeping in mind that in the straightforward case of Bohm diffusion at a linear shock, the maximum energy of electrons scales as $B^{-1/2}$, therefore $E_{\text{syn;cut}}$ is independent of the magnetic field. In our calculations, the non-linear effects induce a weak dependence on magnetic field, as discussed in x 3.

In this paper we compute the synchrotron radiation spectrum limited to X-ray band. The radio emission, being produced by lower energy electrons, with much longer

lifetimes, is affected by the temporal evolution of the supernova remnant, which strongly depends on the environment in which the blast wave propagates.

The X-ray emission is confined to a narrow region behind the shock, whose thickness is determined, depending on the radiating electron energy, by either the diffusion or advection length covered by electrons during their loss time. As we show at the end of next section the contribution to the X-ray radiation from the upstream region is negligible, due to the much lower magnetic field (see Fig. 5 and the corresponding discussion). The thickness of the radiating rim can be estimated by solving the diffusion-convection equation in the downstream plasma: $u_2 (\partial f_e / \partial x) = D \partial^2 f_e / \partial x^2 - f_e =_{\text{syn}}$, where B_2 has been assumed to be spatially constant (i.e. we are neglecting any magnetic damping mechanisms). The solution has the form $f(p; x) / \exp(-x/R_{\text{rim}}(p))$ where $R_{\text{rim}}(p)$ is the spatial scale of the emitting region for electrons with momentum p and is given by (Berezhko & Volk 2004):

$$R_{\text{rim}} = \frac{2D_2 = u_2}{1 + 4D_2 = u_2^2_{\text{syn}}} : \quad (10)$$

The observed thickness of the rim is obtained by correcting the previous expression for projection effects. In the ideal case of a spherical shock, an exponential profile translates into a projected thickness $R_{\text{obs}} \approx 4.6 R_{\text{rim}}$ (Parizot et al. 2006), where R_{obs} is defined as the size of the region over which the observed brightness drops to half of the maximum.

Finally, electrons contribute to gamma ray emission through their ICS of ambient photons. The main contribution to gamma ray emission comes from upscattered dust-processed infrared photons, having a blackbody spectrum with temperature ~ 20 K (Schlegel et al. 1998). Following the instance of the IR + Opt photon background in the interstellar medium (ISM) we assume that the ratio of the optical to infrared energy densities remains ~ 20 , while the energy density of IR light, W_{IR} , is left as a free parameter (in the ISM, $W_{\text{IR}} \approx 0.05 \text{ eV cm}^{-3}$).

The flux and spectrum of ICS photons is calculated by using the exact kernel for ICS, with the full Klein-Nishina (KN) cross section (Rybicki & Lightman 1985). The spectrum is cut off at an energy

$$E_{\text{ICS;cut}} \approx 5 \frac{E_{\text{em;ax}}^2}{\text{TeV}} \frac{p_{\text{h}}}{\text{eV}} \text{ TeV} ; \quad (11)$$

if $E_{\text{em;ax}} \approx 6260 (p_{\text{h}} = \text{eV})^{1/2} \text{ GeV}$ and $E_{\text{ICS;cut}} = E_{\text{em;ax}}$ otherwise. The boundary between the two regimes corresponds to the setting in of the KN regime. For the photon background we adopted here ($p_{\text{h}} \approx 2 \times 10^3 \text{ eV}$), the threshold is at energy $\approx 150 \text{ TeV}$, therefore for the case of RX J1713.7-3946, the cutoff region falls well within the Thomson regime and Eq. (11) applies.

3 RESULTS: RX J1713.7-3946

In this section we describe the results of our calculations for the case of SNR RX J1713.7-3946. A major difficulty in carrying out detailed calculations on this remnant is that neither its distance nor its age are well established. Koyama et al. (1997) infer a distance of $\sim 1 \text{ kpc}$, based on ASCA X-ray observations, while Slane et al. (1999) estimate

a distance of $\sim 6 \text{ kpc}$. Here we adopt the value of 1 kpc , which appears to be supported by some more recent work (Fukuier et al. 2003; Moriguchi et al. 2005) based on the spatial correlation between the remnant and a molecular cloud located at that distance. This estimate was also independently confirmed by Cassam-Chena et al. (2004) based on the comparison between the interstellar absorption as measured using X-ray and radio observations. Since the observed angular size of the remnant is $\sim 6''$, the remnant radius can be estimated to be $R_{\text{SNR}} \approx 10 \text{ pc}$, which would lead to estimate an age of $\sim 1600 \text{ yr}$, consistent with the historical Chinese record of a SN exploded in AD 393 (Wang et al. 1997).

Several authors, based on different arguments, have reached the conclusion that RX J1713.7-3946 is a core-collapse SN of type II/Ib, expanding into a hot and very diluted bubble created by the wind of a massive progenitor star with initial mass between $15 < M < 20 M_{\odot}$ (Berezhko & Volk 2006; Slane et al. 1999; Fukuier et al. 2003; Cassam-Chena et al. 2004). These authors also conclude that the bubble must have a radius of $15 < R_b < 20 \text{ pc}$, hence the shock front of the remnant is most likely still propagating into the low density shocked wind, except perhaps for the SW region where the shock seems to impact the cold and dense shell of unshocked material. This scenario leads to a temperature for the bubble typically $> 10^7 \text{ K}$ (Chevalier & Liang 1989). In order to account for the inhomogeneity of the medium, we adopt here a somewhat lower value of $T_0 = 10^6 \text{ K}$. We checked however that our results are very weakly dependent on the value of the gas temperature at upstream density, as long as it is larger than 10^4 K .

Other uncertainties that affect the results of our calculations concern the density of the background medium, n_0 , and the strength of the background magnetic field (before amplification takes place). Here we adopt $n_0 = 0.12 \text{ cm}^{-3}$, which is somewhat dictated by the fitting to the HESS data. Somewhat larger values of n_0 could be still compatible with HESS observations if a fudge factor is introduced to account for the fact that the gamma ray emission is not homogeneous over the SN shell. Several attempts at measuring the ambient gas density have been made. An upper limit of 2.6 cm^{-3} comes from the molecular hydrogen column density in parts of the SNR without detectable CO emission that can be derived based on NANTEN (Fukuier et al. 2003) measurements (see also Aharonian et al. (2006) for a discussion).

The other existing constraint was inferred by Cassam-Chena et al. (2004) based on the lack of thermal X-ray emission in XMM data. The limit reads $n_0 < 0.02 \text{ cm}^{-3}$. However, it is worth keeping in mind that this limit was derived by assuming that electrons and protons are in thermal equilibrium downstream, but the same authors suggest that this is likely not the case. They also investigate the non-equilibrium case but apparently they used an equal temperature of electrons and protons in this second case as well.

An upper limit of 4500 km/s to the velocity of the ejecta was inferred by Uchiyama et al. (2007) based on a direct measurement of the transient X-ray emitting region. On the other hand a value $u_0 < 1500 \text{ km/s}$ would not allow for acceleration of electrons up to high enough energy to explain the observed X-ray emission. Here we adopt a value of $u_0 = 4300 \text{ km/s}$ necessary to fit the cutoff in the X-ray

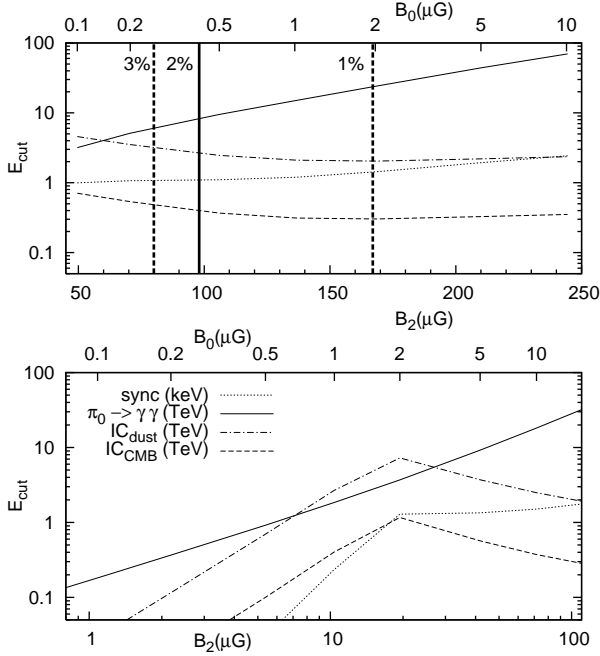


Figure 1. Cutoff energies for photons produced by synchrotron emission (dotted line, in keV), pion decay (solid) and IC scattering (dot-dashed for scattering on IR radiation, dashed for CMB), as a function of the downstream magnetic field B_2 . Also shown on the upper x-axis of both panels is the corresponding value of the background magnetic field B_0 that was used for the calculation. Notice that while the B_2 -scale is logarithmic, the B_0 -scale is arbitrary and built to show the correspondence between B_0 and B_2 . The upper panel shows the case where B_0 is resonantly amplified by the streaming instability. Here the thick vertical lines indicate the solutions having the X-ray rim thickness equal to 1%, 2% and 3% of the SNR radius respectively. In the lower panel we assume no magnetic field amplification, but simple compression of B_0 in the precursor and at the shock. The results in both panels are obtained with $\beta = 3/7$ and $n_0 = 0.12 \text{ cm}^{-3}$, and with the maximum proton momentum determined by the condition $\tau_{\text{acc}}(p_{\text{max}}) = 1600 \text{ yr}$.

spectrum as detected by Suzaku. A lower value of about 3000 Km/s would be needed to fit the ASCA data, but we do not discuss this case any further here, given the superior quality of the Suzaku data.

The model parameters are further constrained by the fact that the magnetic field in the downstream plasma, B_2 , is an output of our calculations, for given B_0 , as it is the result of cosmic ray induced magnetic field amplification and further enhancement by compression in the precursor and at the subshock. The correct solution of the problem is found by not only requiring that the fluxes of observed radiations are fit, but also requiring that B_2 corresponds to the value inferred from the measured thickness of the X-ray rim. For SNR RX J1713.7-3946, we use the data presented in Lazendic et al. (2004) where the authors use a CHANDRA observation at 5 keV to infer the rim thickness in the northwestern region of the SNR. The procedure leads to $R_{\text{obs}} \approx 0.02 R_{\text{SNR}}$ (see their Fig. 9). Clearly this thickness does not lead to an estimate of B_2 if due to damping of the magnetic field (as proposed by Pohlet al. (2005)) rather than to particles' energy losses. Below, we first assume that

the downstream magnetic field can indeed be derived from the extent of the X-ray filaments and then we investigate the consequences of relaxing this constraint.

A first indication of the origin of the observed radiations can be obtained by looking at the cutoff frequencies in the different bands. In the upper panel of Fig. 1 we show the cutoff energies for synchrotron emission (dotted line, in units of keV), π^0 decay (solid line, in TeV) and IC scattering (dash-dotted line for IC on the infrared light and dashed line for IC on the CMB) as given by Eqs. (8), (9) and (11). The plot is obtained for $\beta = 3/7$ and varying B_0 between 0.1 and 10 G (upper x-axis), while the lower x-axis shows the corresponding value of B_2 . The thick vertical solid line shows the solution that provides the central value of the measured rim thickness (corresponding to $B_2 = 100 \text{ G}$) while the dashed vertical lines bound the allowed region corresponding to $1\% < R_{\text{obs}} = R_{\text{SNR}} < 3\%$.

For the range of values of B_0 considered here, it is apparent that IC cannot provide a high enough cutoff energy so as to explain HESS data. The latter require $E_{\text{cut}} > 10 \text{ TeV}$, while the highest value of the IC cutoff energy obtained for scattering on the IR light in the presence of an extremely low background magnetic field ($B_0 = 0.1 \text{ G}$) is 4 TeV. The corresponding cutoff energies for IC on the CMB photons are lower by roughly the ratio of temperatures: $T_{\text{dust}}/T_{\text{CMB}} \approx 7$. The general trend of the IC cutoff energy is to decrease as a function of B_0 (and B_2) because larger values of the magnetic field lead to stronger synchrotron losses and thereby lower maximum energies of the electrons. There are however two subtleties. First, taking into account nonlinear effects in the computation of the acceleration time reduces somewhat the dependence of E_{cut} on the magnetic field, with respect to the expectations of the linear shock analysis. Moreover, for values of B_2 lower than 20 G, the maximum electron energy is determined by the finite age of the remnant rather than by synchrotron losses. Hence, for values of the magnetic field below this threshold, the maximum electron energy increases with increasing magnetic field (because of the more effective diffusion) and reaches a maximum for $B_2 \approx 20 \text{ G}$. This corresponds to the highest possible value of E_{cut} .

It is important to stress that the conclusion that the cutoff frequency for IC falls short of explaining HESS data by about one order of magnitude is independent of arguments related to the normalization of the flux, which we comment upon below.

The cutoff energy for gamma rays produced by π^0 decay is $> 10 \text{ TeV}$ provided $B_0 > (0.3 - 1) \text{ G}$, which interestingly enough is also the region where B_2 is consistent with the thickness of the X-ray rims, if these are interpreted as the result of severe synchrotron losses downstream.

The cutoff energy of synchrotron emitted photons, which, assuming Bohm diffusion, in linear theory would not depend on the value of the magnetic field, now acquires a weak dependence on B_0 , and varies between 1 and 2 keV for the considered range of magnetic field values, granted that $B_2 > 20 \text{ G}$. Things change drastically when B_2 is lower than this threshold and the maximum electron energy is determined by the competition between acceleration time and age of the system, rather than synchrotron losses (lower panel of Fig. 1).

The adopted value $\beta = 3/7$ corresponds to a fraction

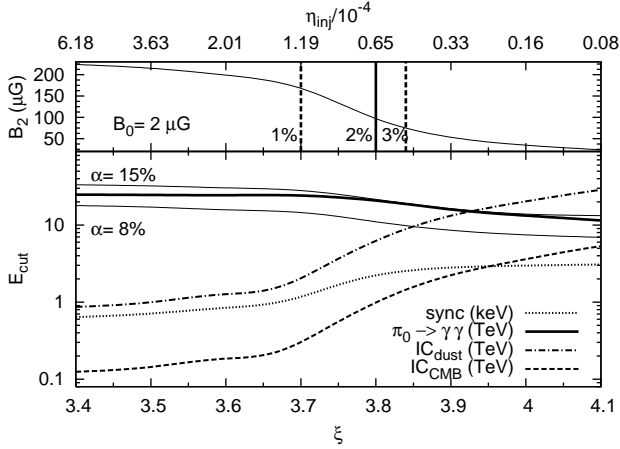


Figure 2. The thick lines in the lower panel show the cutoff frequencies for the radiative processes (just as in Fig. 1) now computed as a function of the injection efficiency, for fixed $B_0 = 2$ G. The thin solid lines show the cutoff frequency for π^0 decay when the maximum proton energy is computed according to the definition on the right of Eq. (1) with $\beta = 0.08$ and 0.15 . The downstream magnetic field, resulting from the amplification and further compression of B_0 , is shown in the upper panel, where the vertical lines have the same meaning as in Fig. 1. The upper x-axis of this panel displays the fraction of injected particles in units of 10^{-4} .

of injected particles $\eta_{inj} = 1.2 \cdot 10^4$. The resulting acceleration efficiency, β , defined as the percentage of the energy flux crossing the shock that ends up in relativistic particles, varies from 68% (for $B_0 = 0.1$ G) to 36% (for $B_0 = 10$ G).

It is very important to notice that the solutions corresponding to the curves in the upper panel of Fig. 1 are characterized by moderately low values of the compression factor in the precursor ($R_{tot} < 12$), despite the high acceleration efficiencies. This result is purely the consequence of the dynamical reaction of the amplified magnetic field on the shock. No turbulent heating has been introduced in these calculations. One may wonder how the results would change if no cosmic ray induced magnetic field amplification were present, so that the magnetic field in the precursor and at the shock would only be produced by compression of a turbulent field at upstream infinity, with $B = B_0$. In this case the turbulent field (assumed to be perpendicular to B_0) is compressed according to $B_2(x) = B_0(u_0 = u(x))$. In the bottom panel in Fig. 1 we show the cutoff energies obtained in this situation (we still assume $\beta = 3.7$). For $0.1 < B_0 < 10$ G, the total compression factor ranges between 14 and 7, and B_2 reaches up to 100 G. Remarkably, the highest value of the maximum energy of gamma rays produced by ICS (on the IR photons) is 7 TeV and is reached for $B_0 = 2$ G ($B_2 = 20$ G). Lower and higher values of B_0 lead to smaller cutoff energy for the ICS emission.

The results of the calculations are very sensitive to the recipe adopted for the injection of cosmic rays from the thermal pool. As discussed in §2.1, we model the injection with the thermal leakage-like model introduced by Blasi et al. (2005). In Fig. 2 we illustrate the dependence of B_2 (upper panel) and of the cutoff energies (lower panel) on the injection parameter η , varying between 3.4 and 4.1 (cor-

responding to $6 \cdot 10^4 < \eta_{inj} < 8 \cdot 10^6$). The upstream magnetic field is $B_0 = 2$ G. The curves are labelled as in Fig. 1, with the addition of two thin solid lines representing the cutoff energy for π^0 decay when the maximum energy of the parent protons is calculated with $\beta = 8\%$ and $\beta = 15\%$ in Eq. (1). The vertical thick solid line in the upper panel shows the solution providing the central value of the measured rim thickness (corresponding to $B_2 = 100$ G) while the dashed vertical lines bound the allowed region corresponding to $1\% < R_{obs} = R_{SNR} < 3\%$.

The cutoff energy for gamma rays due to ICS is again lower than 10 TeV, with the possible exception of ICS on IR light for the highest values of η . For instance, for $\beta = 3.9$ the cutoff energy for ICS is 12 TeV, but in this case the cutoff frequency for pion decay is at the same level. In this limit case the issue becomes the absolute normalization. In any case such situation also corresponds to $B_2 \approx 50$ G, quite lower than inferred from X-ray measurements (compare with the region between the two vertical dashed lines in the upper plot).

The above discussion leads to conclude that there is some degeneracy in the choice of the values of the parameters of this problem. If we try to fit the spectral energy distribution in the X-ray and gamma ray bands and the thickness of the X-ray filaments simultaneously, we find that the best fit is obtained for $1 < B_0 < 3$ G and $3.7 < \beta < 3.85$. The resulting acceleration efficiency varies in the range $20\% < \beta < 60\%$. In Fig. 3 we show a possible solution with $B_0 = 2.6$ G and $\beta = 3.8$. The contribution of π^0 decay to the gamma ray flux is plotted as a thick solid line. The solid curve in the lower energy part represents the synchrotron emission of electrons, superimposed on the recently published Suzaku data (Tanaka et al. 2008). The flux of ICS photons when the target is made of CMB photons is plotted as a dashed line. The ICS on the IR + Opt photons, assumed to have a density equal to the average value in the Galaxy (1 eV cm^{-3}) corresponds to the lower thick dash-dotted line. For illustration purposes, we also plot the contribution of ICS on a IR + Opt background with energy density 200 times larger (higher dash-dotted line). It is worth noticing that while synchrotron emission is always the dominant loss mechanism for electrons, the rate of energy losses due to inverse Compton scattering mainly comes from interaction with the optical photons. On the contrary, the leptonic gamma ray flux in the HESS band is mostly contributed by upscattering of the IR photons.

Fig. 3 shows a few important points: 1) in terms of shape, normalization and position of the cutoff the contribution of π^0 decay provides a satisfactory fit to HESS observations; 2) the ICS on the CMB photons is characterized by too low a normalization and too low cutoff energy; 3) for ICS on the IR + Opt light, the normalization can be raised to the observed flux level only if a very large photon flux is assumed; 4) even in this case the position of the cutoff in the gamma ray spectrum turns out to be below the observed one; 5) while being below the sensitivity limit of EGRET, the predicted fluxes should be observable by GLAST.

As the HESS observations show (Aharonian et al. 2007), the gamma ray spectrum in the TeV region can be fit by a cutoff with shape $\exp[-(E/E_0)]$ with β close to 0.5. As shown here (see also Kelner et al. (2006)), this result is perfectly compatible with the spectrum of gamma rays from

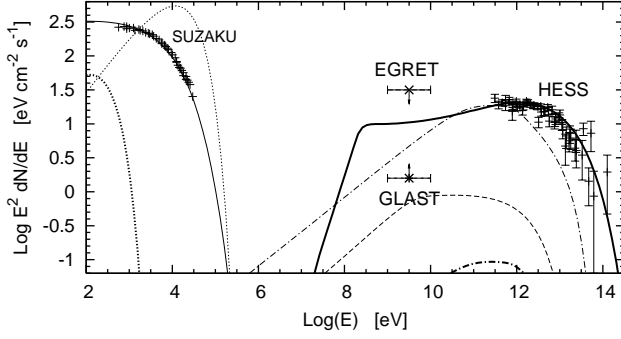


Figure 3. Spatially integrated spectral energy distribution of RX J1713.7-3946 in the hadronic scenario, for $n_0 = 0.12 \text{ cm}^{-3}$, $u_0 = 4300 \text{ km/s}$, $B_0 = 2.6 \text{ G}$, $\beta = 3.8$. The following components are plotted: synchrotron (dotted line) thermal emission (dotted line), Compton scattering with CMB (dashed line) and with Opt+IR background (dot-dashed line). The contribution from pion decay is shown as a thick solid line and corresponds to $p_{p, \text{max}} = 1.26 \cdot 10^5$. HESS data taken from 2003 to 2005 are plotted together with Suzaku data in the X-ray band. Also EGRET upper limit and GLAST sensitivity are shown.

the decay of neutral pions, if the cut-off in the spectrum of the parent protons is exponential.

A few words are in order concerning the maximum momentum of protons. The value of $p_{p, \text{max}}$ that provides the best fit to the data is $1.26 \cdot 10^5 m_p c$, which is obtained when the maximum proton energy is calculated by using the condition of finite size of the accelerator with $\beta = 0.08$ in Eq. (1) (see also Fig. 2). The condition on the age of the remnant would have resulted in a maximum proton energy larger by a factor 2.

A criticism to the scenario just discussed could be raised in that the flux of thermal X-rays plotted in Fig. 3 as a thin dotted line exceeds the Suzaku observations. This is however true only if protons and electrons in the downstream plasma are in thermal equilibrium, while there are reasons to believe that this is not the case (Cassam-Chena et al. (2004)). If one assumes $T_e = 0.01 T_p$ the absence of thermal X-ray emission is naturally explained (thick dotted line in the same plot).

The Suzaku data points are fit extremely well by our calculations: a fact which at least confirms that the shape of the electrons spectrum close to the cut-off is $\propto \exp[-(E/E_{e, \text{max}})^2]$ rather than a simple exponential. In other words, the maximum energy of electrons in this remnant is determined by energy losses, rather than by the finite age of the system. Although not very stringent, this argument suggests that the magnetic field cannot be too low, or otherwise ICS losses would have to be dominant, implying the presence in the remnant of a density of IR photons much larger than in the ISM.

What if the narrow X-ray filaments are due to magnetic field damping or other processes other than severe synchrotron losses? In this case there is no constraint on the strength of the magnetic field at the shock, therefore one may try to test the possibility of fitting the gamma-ray data with the ICS emission of high energy electrons. We carry out the previous calculations, including the magnetic field amplification due to streaming instability but choosing now a large value of the parameter β , so as to reduce the in-

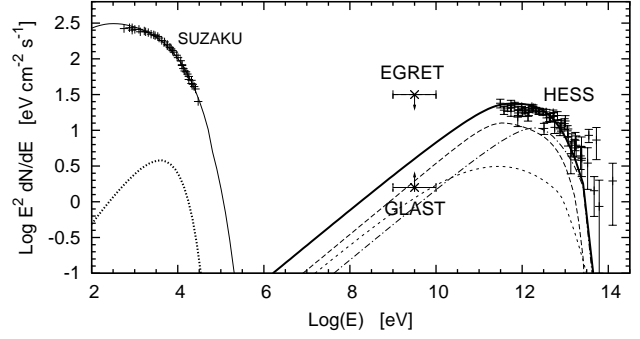


Figure 4. Spatially integrated spectral energy distribution of RX J1713.7-3946 in the leptonic scenario. The following components are plotted: synchrotron (thin solid line) and thermal (thick dotted line) electron emission, ICS component for CMB (dashed line), optical (dotted line) and IR (dot-dashed line) photons, and the sum of the three (thick solid line). The Opt+IR components are assumed to have energy density 24 times the mean ISM value. The other parameters are: $n_0 = 0.01 \text{ cm}^{-3}$, $u_0 = 4300 \text{ km/s}$, $B_0 = 1.5 \text{ G}$ and $\beta = 4.1$. The experimental data are the same as in Fig. 3.

jection. This leads to two main effects: 1) lower efficiency of proton acceleration and 2) correspondingly lower efficiency of magnetic field production.

For the same values for the supernova as above (especially the distance and velocity of the shock), and assuming $n_0 = 0.01 \text{ cm}^{-3}$ and $\beta = 4.1$, we obtain the results illustrated in Fig. 4. These parameters correspond to a fraction of accelerated particles of order $7 \cdot 10^6$ and a cosmic ray energy conversion fraction of 2%. The curves are labelled as follows: the solid and dotted line on the left side of the plot are the synchrotron and thermal electron emission respectively. The thin dashed, dotted and dot-dashed curves are the ICS on the CMB, optical and IR photons respectively, while the solid thick line is the sum of the three. The assumed energy density for the optical and IR radiation is 24 and 12 eV cm^{-3} respectively.

From Fig. 4 we conclude that a fit to HESS data on RX J1713.7-3946 can be obtained within an ICS scenario at the price of: 1) assuming an IR background in the SNR which exceeds the ISM value by a factor 24; 2) neglecting the highest energy data points of HESS.

The first issue has to do with the plateau-like shape of the gamma-ray spectrum in the lower energy part, which cannot be fit unless a second component of the photon background (at higher frequencies) is assumed. This argument was also made by Tanaka et al. (2008).

The second point is due to the fact that despite the small efficiency for proton acceleration, the magnetic field inferred for the downstream plasma is still $\sim 20 \text{ G}$, therefore the maximum energy of electrons is still not large enough to have gamma-ray emission above 10 TeV. Moreover it is worth noting that, in spite of the high energy density assumed for the optical background, i.e. 24 eV cm^{-3} , the synchrotron losses still dominate over the ICS losses because the scattering occurs in the KN limit. As a consequence the spectrum of electrons is cut off as $\exp[-(E/E_{e, \text{max}})^2]$, resulting in a gamma-ray spectrum with a rather sharp cut-off which does not extend to sufficiently high energies to reach HESS highest energy data. This is a point which is often

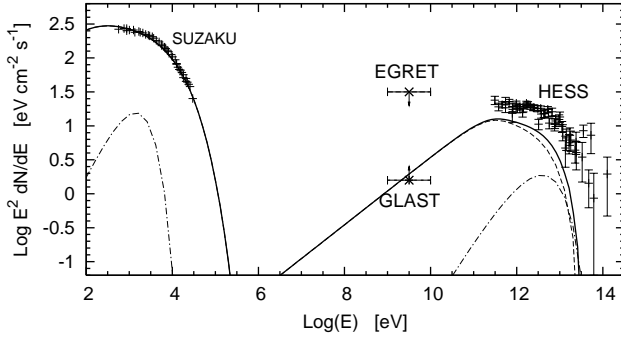


Figure 5. Integrated spectral energy distribution for the leptonic scenario as in Fig. 4. Here only the synchrotron emission and the ICS for CMB are shown, separated in the contributions from the upstream (dot-dashed line) and from the downstream region (dashed line). The solid line is the total contribution.

overlooked in papers investigating the ICS interpretation of the HESS data.

The fluxes shown in Figs. 3 and 4 are obtained by integrating over the emission volume, comprising the upstream and downstream regions. It is instructive to show the emission in the different bands from the upstream and downstream regions separately, since it illustrates some of the non-linear effects discussed above. In order to do that, we concentrate on the case of inefficient acceleration ($\eta = 4:1$) which leads to the leptonic scenario. We stress again that even in this case the magnetic field is generated upstream by the streaming cosmic ray protons and further compressed in the precursor and at the subshock. Moreover, for simplicity we use only the CMB photons as a target for ICS (this is the reason why the predicted fluxes do not fit the HESS data points). The fluxes from downstream (dashed lines) and upstream (dot-dashed lines) are illustrated in Fig. 5. The solid lines represent the total emission, as the sum of the upstream and downstream contributions. For both synchrotron emission and ICS the main contribution comes from the downstream region, at almost all photon energies. For synchrotron emission, the relative ratio of the integrated emission from upstream and downstream is larger than that calculated in the test particle case (see for instance Zirakashvili & Aharonian (2007)) because particles upstream feel a smaller mean magnetic field in the non-linear case, hence the upstream synchrotron flux is smaller than in the test particle case. The contribution of electrons to ICS from the upstream region is also smaller than the corresponding downstream contribution, although in the cutoff region the former provides an appreciable fraction of the total gamma ray flux.

We conclude the review of the results of our calculations with a discussion of the integrated spectrum of accelerated protons and electrons. These are shown (multiplied by p^2) in Fig. 6 for both the hadronic (thick lines) and the leptonic scenario (thin lines). The break in the electron spectra is due to the onset of synchrotron losses in reaching equilibrium. In both scenarios the maximum energy of electrons is due to the balance between acceleration and synchrotron losses, although in the leptonic case the situation is borderline with the age of the system becoming comparable with the time for synchrotron losses. The most important comment on the spectra of accelerated particles, especially protons, is the

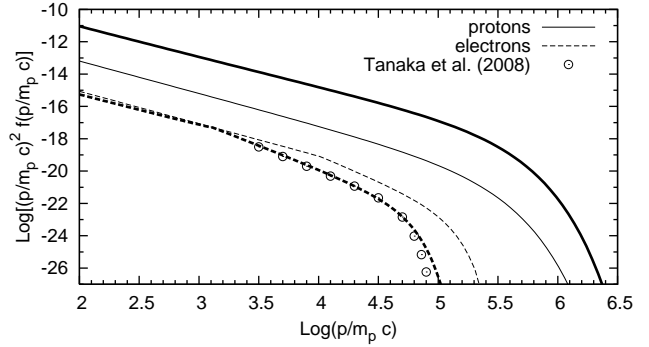


Figure 6. Spatially integrated spectra for accelerated protons (solid lines) and electrons (dashed lines) as functions of momentum. Thick and thin lines refer to the hadronic dominated scenario (see Fig. 3) and leptonic dominated scenario (see Fig. 4) respectively. Circles represent the electron distribution as obtained by Tanaka et al. (2008).

concavity of the spectra which appears to be barely visible. A standard non-linear calculation with the shock parameters adopted here would lead to strongly modified (concave) spectra. The reduction of this effect is a crucial consequence of the dynamical reaction of the amplified magnetic field on the precursor, which leads to a reduction of the spectral concavity (see discussion in §2.2). The cutoff in the spectrum of accelerated protons is due to finite acceleration time. Fig. 6 also provides a visual estimate of the value of K_{ep} as it appears in Eq. 5, namely $K_{ep} = 6 \times 10^5$ for the hadronic scenario and 1.4×10^2 for the leptonic one. Finally, in Fig. 6 we also compare our electron energy spectrum, as obtained in the hadronic scenario, with that derived by Tanaka et al. (2008) (see their Fig. 12) directly from the Suzaku X-ray data (circle points). The two spectra are in good agreement, with the possible exception of the few data points at the highest energies.

4 CONCLUSIONS AND CRITICAL DISCUSSION

The detection of high energy gamma rays from SNRs has long been considered as the most important tool to test the supernova paradigm for the origin of galactic cosmic rays. We now have a couple of positive gamma ray detections in the 1–100 TeV energy range, but it remains unclear whether this emission is of hadronic or leptonic origin. A hadronic origin would point to the acceleration of cosmic rays up to energies close to the knee, which is the main motivation for this work.

We investigated the problem in the context of the non-linear theory of particle acceleration at SNR shocks, including the dynamical reaction of the accelerated particles, the generation of magnetic fields as due to streaming instability excited by cosmic rays, and the dynamical reaction of these self-generated fields on the plasma. We specialized our calculations to the SNR RX J1713.7-3946. Previous attempts to carry out similar calculations did not include the magnetic field amplification (which was input by hand so as to fit the data) and its dynamical reaction. The latter is crucial to reduce the compression factors to the levels needed to explain

the few available observations (Caprioli et al. 2008a), while in previous work on the topic, this problem was faced by invoking turbulent heating (see for instance Berezhko & Volk 2006)).

The non-linear calculations are applied to two cases with very different acceleration efficiency. In the first scenario, the shock accelerates a fraction 10^{-4} of the incoming particle flux, which results in large acceleration efficiency and effective magnetic field amplification through resonant streaming instability. This scenario provides a benchmark for a hadronic interpretation of the HESS gamma ray observations of RX J1713.7-3946. In the second scenario a fraction 10^{-6} of the incoming particle flux through the shock gets accelerated. This serves as a model for a leptonic origin of the HESS data on RX J1713.7-3946.

The main discrimination between the two scenarios resides in the strength of the magnetic field at the shock: efficient cosmic ray acceleration also leads to the generation of magnetic field upstream of the shock which by compression translates into a downstream field of $B_2 \sim 100$ G, compatible with the value which has been inferred from the interpretation of the morphology of the X-ray emission as due to synchrotron losses. The second scenario requires that the magnetic field is very weakly amplified (if at all), so that $B_2 \sim 15-25$ G. In this case the X-ray morphology is interpreted as a result of damping of the magnetic field in the downstream plasma (Pohl et al. 2005).

In the following we discuss these two scenarios in terms of their problems and virtues, which also leads us to comment on the origin of the X-ray filaments.

Our calculations show that for the parameters typically adopted for RX J1713.7-3946, and assuming $\beta = 3/7$ for the injection, particle acceleration of protons works efficiently. X-ray and gamma ray data can be fit very well within this approach, and the strength of the downstream magnetic field turns out to describe well the brightness profile of the X-ray emission without further adjustments. The cutoff in the gamma ray emission leads to conclude that a cutoff in the parent proton spectrum is at 10^5 GeV. We stress that this is the cutoff in the proton spectrum which is being accelerated at the present time, while the highest energy which can be achieved in a SNR is reached at the very beginning of the Sedov phase. During the Sedov phase, particles which reached higher energies at previous times escape the system from upstream (and indeed these are the only particles which are allowed to leave the system from upstream). The shape of the X-ray spectrum is taken from the recent Suzaku observations of RX J1713.7-3946 (Tanaka et al. 2008), which lead to a cutoff energy in the X-ray spectrum requiring a shock velocity of 4300 km/s within the framework of our model. For Bohm diffusion the energy of the X-ray cutoff is very weakly dependent on the magnetic field strength in the shock region (in fact in linear theory it would have been independent of B). In this scenario the IC contribution from high energy accelerated electrons is negligible compared with the contribution of 0 decays, unless an unreasonably large energy density of target IR light is adopted.

The best fit is achieved by using a density of the upstream gas of $n_0 = 0.12$ cm $^{-3}$. The implications of this result are far reaching and deserve some discussion: as shown in Fig. 3 the emission expected from the gas behind the shock as a result of thermal bremsstrahlung emission of elec-

trons exceeds the observed flux by a factor ~ 6 . This conclusion could be also derived based on simpler calculations, as done by Katz & Waxman (2008). However, as also argued by Cassam-Chena et al. (2004), the electrons and protons in this SNR are not expected to be in thermal equilibrium because of the relatively low density of the medium. This possibility is also discussed by Ghavamian et al. (2007), who find that for a remnant with velocity 3000 km/s the ratio of the electron to proton temperature is ~ 0.02 and scales as V_s^{-2} (recall however that these conclusions were obtained in the context of linear calculations, and could be even stronger if the non-linear effects are taken into account). We showed that such a temperature ratio would lead to predict a thermal X-ray emission well below the sensitivity of Suzaku and ASCA. On the other hand, although the age of this remnant is too short to allow Coulomb scattering to equilibrate electrons and protons downstream, one should check that Coulomb scattering acting for ~ 1600 years does not heat electrons enough (about 1 keV) to excite lines in iron atoms, which would then become easily visible on top of the synchrotron emission (see for instance Ellison et al. (2007) for a discussion of this effect).

Katz & Waxman (2008) also criticized the hadronic scenario based on the lack of an excess gamma ray emission in the direction in which, according to Cassam-Chena et al. (2004) the shock appears to have impacted a nearby molecular cloud, where the target density for pp collisions should be higher. As simple as this inference may sound, it is not that straightforward: the gas in the molecular cloud is expected to be mostly neutral, a fact that has at least two important consequences. First, only the ionized component takes part in the acceleration process (recall that in order to be scattered back towards the shock from downstream, incoming particles should be ionized within a few times the shock thickness). This implies that the efficiency of particle acceleration in the proximity of the molecular cloud could be much lower than in less dense parts of the surrounding medium. Moreover, in a mostly neutral medium, the Alfvénic turbulence on which efficient particle acceleration relies can be effectively damped, thereby leading to a lower maximum energy of accelerated particles. These two instances show that having a dense target for pp collisions does not necessarily imply that there should be a larger gamma ray flux from 0 decay.

As already stressed, the actual trademark of the hadronic scenario discussed above is the prediction that the downstream magnetic field in RX J1713.7-3946 is $B_2 \sim 100$ G, which would imply that the filaments observed in X-rays are due to severe synchrotron losses of accelerated electrons. Pohl et al. (2005) argued that a narrow region of X-ray emission could also be due to damping of the magnetic field downstream of the shock. The argument was also adopted by Katz & Waxman (2008) in order to suggest that HESS gamma rays must be of leptonic origin. Katz & Waxman (2008) also quote the results of Rothenflug et al. (2004) on SN 1006 to stress that filamentary structures are observed also in the radio and not only in X-rays, therefore the filaments cannot be due to synchrotron losses. It should be noticed, however, that Rothenflug et al. (2004) use their data to reach the opposite conclusion. In fact Rothenflug et al. (2004) plot the spatial profiles of the radio and X-ray emission, which show that the radio emission profile has only a shallow bump, when compared with

the pronounced peak in the X-ray brightness. We should recall that the thickness of the damping region, as correctly proposed by Pohl et al. (2005), is determined by using the convection equation for the waves, with no generation terms and only a damping term. This trivially leads to a solution which is an exponential in the spatial coordinate with a cutoff scale which defines the damping scale. It is worth reminding that the exponential shape is the very reason why one should expect a filament. In order to avoid that an equally pronounced filamentary structure appears in radio, Pohl et al. (2005) are forced to assume that the field has a residual large scale component which is not affected by the damping: the radio emission then comes from lower energy electrons propagating in this residual field. This solution appears to us rather untuned, a limitation that should be kept in mind when discussing the damping explanation of the X-ray morphology. This limitation is probably even more serious in the case of RX J1713.7-3946, where the X-ray emitting region is comparatively broader and it is not very easy to explain it with the damping models proposed by Pohl et al. (2005) (see Eqs. (7) and (12) of their paper), although there are many parameters in their formulae that can be appropriately tuned.

In our opinion, a rather serious concern about a hadronic origin of the HESS gamma ray emission, and indeed about this remnant being an efficient cosmic ray accelerator, is the low value of K_{ep} predicted by the non-linear theory. Our calculations lead to $K_{ep} \approx 10^4$, which is much lower than the value inferred from direct measurement of the electron spectrum in the 10 GeV energy region, at the Earth. At first sight one should conclude that if the gamma radiation detected by HESS is of hadronic origin, then electrons should have a different origin, but a dedicated investigation of the problem should be planned to address this issue, since the very problem of electron escape from the remnant needs to be carefully addressed. One obvious warning against easy conclusions in this respect is that the value of K_{ep} measured at the Earth is not the same as inferred for a single SNR at a given age. It is rather an average over the temporal evolution of a remnant and a sum over the many SNRs that contribute a flux at any given time. In fact K_{ep} is in general a function of time for a SNR, and it is possible that low energy electrons are more effectively produced at later times when proton acceleration and magnetic field amplification become less efficient, and probably there is no appreciable gamma ray emission due to pp scattering.

Now we discuss our attempt to fit the HESS data with a leptonic model. We stress that the calculations carried out here are exactly the same as described above, with the only difference that we assume a larger value for the injection parameter, chosen here to be $\eta = 4:1$ (corresponding to a fraction of accelerated particles $\approx 10^{-6}$). The generation of magnetic field by streaming instability is also kept in the calculations, although the predicted field strength is clearly much lower than in the previous case.

As shown in Fig. 4, a fit to the combined HESS and Suzaku data is possible if the highest energy HESS data points are ignored. The cosmic ray acceleration efficiency corresponding to this solution is $\approx 2\%$. The magnetic field found as a result of streaming instability and further compression in the precursor and at the subshock is ≈ 20 G and the cutoff energy of the electrons is still determined by

energy losses. This is an important point, because the cutoff in the electron spectrum is super-exponential (namely $\propto \exp[-(E/E_{cut})^2]$) only if the rate of losses is $\propto E^2$. If the maximum energy of electrons is determined by the finite age of the accelerator, then an exponential cutoff should be expected. The two situations reflect in profoundly different X-ray spectra in the cutoff region. As seen in Figs. 3 and 4, the Suzaku data are well fit by an electron spectrum with a super-exponential cutoff.

The fit illustrated in Fig. 4 has two problems, typical of leptonic models: 1) the nearly flat region in the HESS data cannot be well fit by using CMB photons alone as the target for ICS, as also discussed by Tanaka et al. (2008). In order to solve this problem, a population of IR photons needs to be assumed, with energy density ≈ 20 times larger than in the ISM. We consider this as a problematic aspect of the leptonic model, since this population of photons should be introduced ad hoc, without a proper independent physical motivation. 2) The highest energy data points in the HESS data cannot be fit with ICS of electrons. These data points have been curiously ignored in some of the previous literature on the topic, probably because of their relatively large error bars. It is however not easy to imagine how the highest energy data point, at $E \approx 100$ TeV may disappear. Future observations of this remnant in the multi-TeV range will tell us if this might be the case.

Figs. 3 and 4 clearly show that a major discrimination power between the two scenarios can be achieved with GLAST. In the region $1-100$ GeV, the two scenarios imply a flux which is different by about one order of magnitude. A different conclusion was reached by Yamazaki (2008), due to an oversimplified treatment of particle acceleration in the non-linear regime, which ignored several effects (magnetic dynamical reaction, turbulent heating) leading to much less concave spectra of accelerated protons.

ACKNOWLEDGMENTS

We are grateful to Damiano Caprioli and Gamil Cassam-Chenai for their precious comments. We are also grateful to the anonymous referee for the insights that contributed to improve the paper. This work was partially supported by INAF (under grant PRIN-2005), by MIUR (under grant PRIN-2006), by ASI through contract ASI-INAF I/088/06/0 and (for PB) by the US DOE and by NASA grant NAG 5-10842. Fermilab is operated by Fermi Research Alliance, LLC under Contract No. DE-AC02-07CH11359 with the United States DOE.

REFERENCES

- Aharonian, F., et al. (H.E.S.S. Collaboration), 2007, *A & A*, 464, 235
- Aharonian, F., et al. (H.E.S.S. Collaboration), 2006, *A & A*, 449, 223
- Amato, E., and Blasi, P., 2005, *MNRAS Lett*, 364, 76
- Amato, E., and Blasi, P., 2006, *MNRAS*, 371, 1251
- Amato, E., and Blasi, P., 2008, *MNRAS*, submitted (astro-ph/0806.1223)
- Ballet, J., 2006, *A dv. Sp. Res.*, 37, 1902

- Bam ba, A., Yam azaki, R., Yoshida, T., Terasawa, T., Koyam a, K., 2005, *ApJ*, 621, 793
- Bam ba, A., Yam azaki, R., Ueno, M. & Koyam a, K., 2003, *ApJ*, 589, 827
- Bell, A. R., 2004, *MNRAS*, 352, 550
- Berezhko, E. G., Volk, H. J., 2006, *A & A*, 451, 981
- Berezhko, E. G., Volk, H. J., 2004, *A & A*, 419, L27
- B lasi, P., Am ato, E. & Caprioli, D., 2007, *MNRAS*, 375, 1471
- B lasi, P., Gabici, S. & Vannoni, G., 2005, *MNRAS*, 361, 907
- Caprioli, D., Am ato, E., B lasi, P., & Vietri, M., 2008, *ApJ Lett*, 679, 139
- Caprioli, D., Am ato, E., B lasi, P., & Vietri, M., *MNRAS*, in preparation
- Cassam -Chena , G., Decourchelle, A., Ballet, J., et al. 2004, *A & A*, 427, 199
- Chevalier, R. A., Liang, E. P., 1989, *ApJ*, 344, 332
- Ellison, D. C., and Vladimirov, A., 2008, *ApJ Lett*, 673, 47
- Ellison, D. C., Patnaude, D. J., Slane, P., B lasi, P., and Gabici, S., 2007, *ApJ*, 661, 879
- Fukui, Y., Moriguchi, Y., Tamura, K., et al. 2003, *PASJ*, 55, L61
- Ghavami, P., Lam ing, J. M. & Rakowski, C. E. 2007, *ApJ Lett*, 654, 69
- Giacobone J. and Jokipii J. R., 2007, *ApJ Lett*, 663, 41
- Katz, B. & Waxman, E., 2008, *J. Cosm ology Astropart. Phys.*, 1, 18
- K ehner, S. R., Aharonian, F. A. and Bugayov, V. V., 2006, *Phys. Rev. D*, 74, 034018
- Koyam a, K., Kinagasa, K., Matsuzaki, K., et al., 1997, *PASJ*, 49, L7
- Lazendic, J. S., Slane, P. O., Gaensler, B. M., Reynolds, S. P., Pucinsky, P. P., and Hughes, J. P. 2004, *ApJ*, 602, 271
- Lazendic J. S., Slane, P. O., Gaensler, B. M., Pucinsky, P. P., Hughes, J. P., Galloway & D. K., Crawford, F., 2003, *ApJ Lett*, 593, 27
- Moriguchi, Y., Tamura, K., Tawara, Y., et al. 2005, *ApJ*, 631, 947
- M orlino, G., Am ato, E., B lasi, P., 2008, in preparation
- Parizot, E., Marcolini, A., Ballet, J. and Gallant, Y. A., 2006, *A & A*, 453, 387
- Pohl, M., Yan, H. & Lazarian, A., 2008, *ApJ Lett*, 626, 101
- Rothen ug, R., Ballet, J., Dubner, G., Giacomini, E., Decourchelle, A., and Ferrando, P., 2004, *A & A*, 425, 121
- Radiative Processes in Astrophysics*, Wiley-Interscience, 1st edition (March 26, 1985)
- Uchiyama, Y. & Aharonian, F., 2008, *ApJ Lett*, 677, 105
- Uchiyama, Y., Aharonian, F., Tanaka, T., Takahashi, T. & Mada, Y., 2007, *Nature*, 449, 576
- Uchiyama, Y., Aharonian, F. & Takahashi, T., 2003, *A & A*, 400, 567
- Schlegel, D. J., Finkbeiner, D. P. & Davis, M., 1998, *ApJ*, 500, 525
- Skilling, J., 1975, *MNRAS*, 173, 255
- Slane, P., Gaensler, B. M., Dame, T. M. et al., 1999, *ApJ*, 525, 357
- Tanaka, T., et al., Preprint arXiv:0806.1490
- Tatische, V., et al., Preprint arXiv:0804.1004
- Vink, J. & Lam ing, J. M., 2003, *ApJ*, 584, 758
- Yamazaki, R., Kohri, K., and Katagiri, H., Preprint arXiv:0806.3303
- Wang, Z. R., Qu, Q.-Y., & Chen, Y., 1997, *A & A*, 318, L59
- Zirakashvili, V. N. & Ptuskin, 2008, Preprint arXiv:0807.2754
- Zirakashvili, V. N. & Aharonian, F., 2007, *A & A*, 465, 695